Article

TRANSPARENT PROCESS

THE EMBO JOURNAL

Membrane protrusion powers clathrin-independent endocytosis of interleukin-2 receptor

Cyril Basquin[1,2,‡], Michaël Trichet[3,†], Helena Vihinen[4,†], Valérie Malardé[1,2,§,†], Thibault Lagache[5,2,†], Léa Ripoll[1,2,¶], Eija Jokitalo[4], Jean-Christophe Olivo-Marin[5,2], Alexis Gautreau[6] & Nathalie Sauvonnet[1,2,§,*]

Abstract

Endocytosis controls many functions including nutrient uptake, cell division, migration and signal transduction. A clathrin- and caveolin-independent endocytosis pathway is used by important physiological cargos, including interleukin-2 receptors (IL-2R). However, this process lacks morphological and dynamic data. Our electron microscopy (EM) and tomography studies reveal that IL-2R-pits and vesicles are initiated at the base of protrusions. We identify the WAVE complex as a specific endocytic actor. The WAVE complex interacts with IL-2R, via a WAVE-interacting receptor sequence (WIRS) present in the receptor polypeptide, and allows for receptor clustering close to membrane protrusions. In addition, using total internal reflection fluorescent microscopy (TIRF) and automated analysis we demonstrate that two timely distinct bursts of actin polymerization are required during IL-2R uptake, promoted first by the WAVE complex and then by N-WASP. Finally, our data reveal that dynamin acts as a transition controller for the recruitment of Arp2/3 activators required for IL-2R endocytosis. Altogether, our work identifies the spatio-temporal specific role of factors initiating clathrin-independent endocytosis by a unique mechanism that does not depend on the deformation of a flat membrane, but rather on that of membrane protrusions.

Keywords actin; cytokine receptor; dynamin; protrusion; wave regulatory complex

Subject Categories Membrane & Intracellular Transport

DOI 10.15252/embj.201490788 | Received 12 December 2014 | Revised 27 May 2015 | Accepted 27 May 2015 | Published online 29 June 2015

The EMBO Journal (2015) 34: 2147–2161

Introduction

Endocytosis is a crucial mechanism that eukaryotic cells use to internalize, both actively and specifically, multiple components. Besides the entry of nutrients, endocytosis is involved in many processes, such as cell migration, division, signalling, differentiation and immune response (Sigismund *et al*, 2012). Over the years, different endocytic pathways have been identified. So far, the best studied pathway is clathrin-dependent endocytosis, involving many well-characterized factors (Mousavi *et al*, 2004). In this process, the cargos are recruited into clathrin-coated pits initiated from a flat membrane that then form clathrin-coated vesicles (Harding *et al*, 1983; McMahon & Boucrot, 2011). Several clathrin-independent routes have been uncovered; however, their molecular mechanisms are not fully understood (Howes *et al*, 2010b; Sandvig *et al*, 2011).

Cytokine receptors, like IL-2R, were among the first physiological examples of cargos taken up by a clathrin-independent mechanism (Subtil *et al*, 1994; Lamaze *et al*, 2001; Sauvonnet *et al*, 2005). These receptors include the β-chain of the interleukin-2 and interleukin-15 receptors (IL-2Rβ) and the common cytokine γ-chain (IL-2Rγc) of the receptors for interleukins 2, 4, 7, 9, 15 and 21. Upon cytokine stimulation, they induce signalling cascades promoting cell proliferation in the immune response (Gaffen, 2001). These cytokine receptors can be internalized constitutively, that is independently of the ligand in various cell types (Hémar *et al*, 1995; Subtil *et al*, 1997), suggesting a widespread mechanism. Once internalized, the receptors are sorted into lysosomes where they are degraded (Hémar *et al*, 1994, 1995). Thus, endocytosis tightly controls their ability to transduce the proliferation signal (Gesbert *et al*, 2004) and further insight into the endocytosis process is crucial to fully understand cytokine receptor functioning.

As this process does not require known membrane coat components, such as clathrin and caveolin (Lamaze *et al*, 2001; Sauvonnet *et al*, 2005), an important issue arises regarding the mechanism of

1 Unité de Biologie des Interactions Cellulaires, Institut Pasteur, Paris, France
2 CNRS UMR3691, Paris, France
3 Sorbonne Universités, UPMC Univ Paris 06, CNRS, Institut de Biologie Paris-Seine (IBPS), FR3631, Electron Microscopy Facility, Paris, France
4 Electron Microscopy Unit, Institute of Biotechnology, University of Helsinki, Helsinki, Finland
5 Unité d'Analyse d'Images Biologiques, Institut Pasteur, Paris, France
6 Laboratoire de Biochimie, Unité Mixte de Recherche 7654 Ecole Polytechnique Centre National de la Recherche Scientifique, Palaiseau, France
*Corresponding author. Tel: +33 145688433; E-mail: nathalie.sauvonnet@pasteur.fr
†These authors contributed equally to this work
‡Present address: Institut Jacques Monod, Equipe de Polarité Cellulaire dans le Développement et l'évolution, CNRS, UMR 7592, Paris, France
§Present address: Unité de Pathogénie Microbienne Moléculaire, Institut Pasteur, Paris, France
¶Present address: Institut Curie, and Unité Mixte de Recherche 144, Centre National de la Recherche Scientifique, Paris, France

plasma membrane remodelling involved in IL-2R endocytosis. Another key question addresses the morphology of the pit, vesicle and intracellular carriers containing IL-2R, for which no data are available. In contrast, the knowledge of this endocytic process is more advanced at the molecular level. Indeed, we previously identified a dozen factors implicated in IL-2R endocytosis, including dynamin, actin and related factors, such as cortactin, N-WASP, Arp2/3, PI3K, Vav2, Rac1 and PAKs (Sauvonnet *et al*, 2005; Grassart *et al*, 2008, 2010; Basquin & Sauvonnet, 2013; Basquin *et al*, 2013). Many of these factors are also involved in clathrin-mediated endocytosis, yielding little insights into the unique mechanism of clathrin-independent endocytosis. However, we have demonstrated that common factors, like N-WASP and cortactin, are regulated differently depending on the mechanism. During IL-2R internalization, PI3K interacts with the receptor and activates Vav2, which then induces Rac1 and Paks. This in turn enhances the association of cortactin-N-WASP, thereby promoting actin polymerization most likely when dynamin is recruited (Sauvonnet *et al*, 2005; Grassart *et al*, 2008, 2010; Basquin & Sauvonnet, 2013; Basquin *et al*, 2013). The present model proposes that all of these factors regulate the last step of endocytosis, the vesicle scission from the plasma membrane. However, validation of this hypothesis requires dynamic data. Besides this current model, nothing is known regarding the initiation of the IL-2R pit and vesicle at either the molecular or the morphological level. In this study, we investigated the structures of the IL-2R-containing pits and vesicles and their formation using ultrastructural data, combined with biochemical experiments and dynamic image analysis.

Results

Morphology of IL-2R-intracellular carriers

The main goal of this study was to obtain structural data to better understand IL-2R endocytosis. To characterize the morphology of membrane and intracellular carriers during all the stages of endocytosis, we performed a cell surface immunogold labelling of IL-2R. We incubated cells at 37°C for several time points to allow for endocytosis, fixed them and observed them by transmission electron microscopy (TEM). As IL-2R internalization occurs in several cell types, constitutively or ligand induced, we decided to use Hep2β cells, a human epithelial cell line stably expressing IL-2Rβ (Grassart *et al*, 2008) to address the constitutive endocytosis. We used Kit225 cells, a human T-cell line expressing the endogenous high-affinity IL-2R, to study the IL-2-induced endocytosis (Basquin *et al*, 2013). After a brief labelling at 4°C of IL-2Rβ (using an antibody targeting IL-2Rβ (Subtil *et al*, 1994) and protein A-gold), cells were incubated for a sufficient time at 37°C (7 min for Kit225 and 12 min for Hep2β) to allow the observation of intracellular vesicles and endosomes bearing IL-2R. TEM observations of ultrathin sections (70 nm) showed a specific labelling of IL-2Rβ, since cells incubated with protein A-gold alone showed very rarely gold particles compared to those incubated with the antibody and protein A-gold (Supplementary Fig S1). TEM data show the uptake of IL-2R in three endocytic compartments in both cell lines (Fig 1). Indeed, we observed IL-2Rβ in vesicles of ovoid shapes having sizes from 40 to 180 nm (mean of diameter 95 nm ± 34 nm, Fig 1A, B, D, E and I), in early endosomes (Fig 1C and F) and in multivesicular bodies (Fig 1C, G and H). These first ultrastructural data show the different steps of IL-2Rβ endocytosis and reveal the internalization of the receptor into small vesicles and its further trafficking to early and late endosomes, as proposed previously (Hémar *et al*, 1995; Basquin *et al*, 2013). Moreover, the distribution of IL-2Rβ in the endocytic compartments was equivalent in both Hep2β and Kit225 cells, showing the same intracellular trafficking of the receptor in both cell lineages, epithelial and lymphoid, respectively. Since all vesicles seen were smaller than 200 nm, our data also show that IL-2Rβ does not enter by a macropinocytic pathway (Lim & Gleeson, 2011). In addition, the shape of these vesicles does not fit with caveolae or with the complex tubulovesicular ring-shaped CLIC morphology (Howes *et al*, 2010a), both of which use a clathrin-independent pathway. Thus, these first ultrastructural data indicate that the endocytic vesicle harbouring IL-2R is morphologically distinct from clathrin-independent endocytic carriers reported thus far.

The IL-2R-containing pit is localized at the base of membrane protrusions

To obtain data regarding the pit and vesicle initiation at the morphological level, we performed the same experiment as for Fig 1, but incubated the cells only briefly at 37°C (2 min for Kit225 and 7 min for Hep2β) to avoid the complete endocytosis of IL-2R. Strikingly, in Hep2β cells, we saw that IL-2Rβ localized on or near protrusions (Fig 2A–C, I, J, M and N). In order to quantify the relevance of this observation, we analysed all gold beads, representing IL-2Rβ, at the plasma membrane and measured with ImageJ the distance to the nearest protrusion observed (Fig 2I). As a control, we also analysed the localization of clathrin-coated pits (CCP) and transferrin (Tf), a cargo using the clathrin-mediated route (Fig 2D and I, Supplementary Fig S2A). We defined five classes of locations with respect to protrusions (Fig 2I): on protrusion, at its base, 100–300 nm, 300–500 nm and > 500 nm from the next protrusion. Quantification of the data shows that 79% of IL-2Rβ is close to protrusions (< 300 nm) at the plasma membrane, while this association is poorly observed with clathrin-coated pits or Tf (42%, Fig 2I, Supplementary Fig S2B). This association of IL-2R close with protrusions does not depend on clathrin because its depletion by siRNA (siRNA CHC) does not change IL-2R distribution (Supplementary Fig S2C–E). Interestingly, we observed the same striking distribution of the receptor close to protrusion in T cells endogenously expressing IL-2R (Kit225) (Fig 2E–H and O). This association of IL-2R with protrusions was not enhanced by the ligand IL-2 (75% (-IL-2) or 79% (+IL-2) Fig 2O). To better characterize the IL-2R pit and vesicle formation, we decided to clarify the role of dynamin, as this GTPase is an essential actor of IL-2R uptake (Lamaze *et al*, 2001) (inhibition up to 80% in dynamin 2-depleted cells (Supplementary Fig S3)). Immunogold labelling and TEM observations of cells depleted for dynamin 2 showed IL-2Rβ in unconstricted pits (U-shape pits, Fig 2L) or in long tubular pits still connected to the plasma membrane (Fig 2K), as was reported for CCP (Damke *et al*, 1994; Macia *et al*, 2006; Wu *et al*, 2010). This result strengthens the importance of dynamin in the last stage of endocytosis to drive the scission of the IL-2Rβ-containing vesicle. However, dynamin 2 is not required for the enrichment of IL-2Rβ to membrane protrusions,

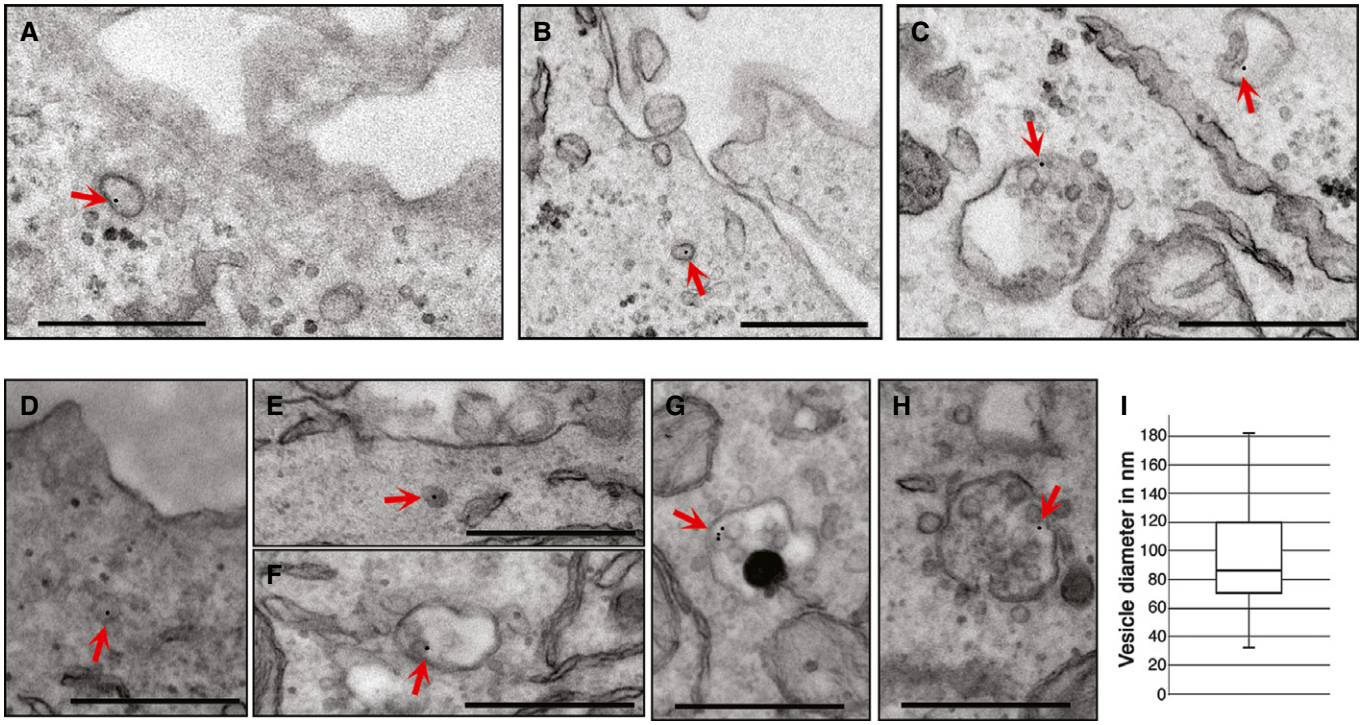

Figure 1. Morphology of IL-2R intracellular carriers.

A–H Hep2β cells or Kit225 cells were incubated at 4°C with an anti-IL-2R antibody and then with protein A coupled to 10-nm gold beads. Endocytosis was enabled by incubating the Hep2β cells for 12 min (A–C) or the Kit225 cells for 7 min (D–H) at 37°C. Cells were fixed and embedded in epoxy resin, and sections were analysed by TEM. Inside the cells, IL-2R can be seen in small endocytic vesicle (A, B, D, E), in early endosomes (C, F) and in multivesicular bodies/late endosomes (C, G, H). Scale bar represents 500 nm. Arrows show IL-2R-containing vesicles, early or late endosomes.

I As carrier vesicles containing IL-2R have an ovoid shape (A, B), both the larger and the minor side of the vesicle were quantified using ImageJ and diameter sizes are presented in a boxplot (four experiments, 50 diameters counted).

as IL-2R-pits (unconstricted or long tubules) are located at the base of protrusions (Fig 2K, L and P). Further analysis of all EM data revealed that most of the pits having IL-2Rβ are seen at the base of such membrane protrusions (Fig 2A–C, E–H and J). All these data suggest the importance of these protrusions in pit initiation. In order to observe the 3D structure of pits containing IL-2Rβ, we performed electron tomography. First, we observed that IL-2Rβ is located in small invaginations at the base of protrusions (Fig 2M, Supplementary Movie S1). At a later stage of endocytosis, once the neck is tight, IL-2Rβ is located in not completely spherical vesicles at the base of protrusions (Fig 2N, Supplementary Movie S2). Altogether, these ultrastructural studies of IL-2Rβ reveal that the receptor is mainly located in protrusion-rich regions of the plasma membrane (Fig 2) and that these pits and vesicles are initiated at the base of such structures. These results are in marked contrast with the current knowledge about the initiation of endocytosis starting with the invagination of flat membrane (Harding *et al*, 1983).

The WAVE complex drives IL-2R close to protrusions

We next searched for the factor promoting the association of IL-2Rβ with these protrusions. Branched actin polymerization is known to be the driving force behind membrane extensions. The WAVE complex is a nucleation-promoting factor activating the actin-related proteins 2 and 3 (Arp2/3) complex, inducing actin polymerization and membrane protrusion (Oikawa *et al*, 2004; Steffen *et al*, 2004). This prompted us to investigate the role of Arp2/3 and the WAVE complexes in IL-2Rβ endocytosis. First, we confirmed that Arp2/3 activation was required for IL-2Rβ, as treatment with CK-666 (a specific Arp2/3 inhibitor) strongly affected IL-2Rβ uptake (90% of inhibition, Supplementary Fig S4A). Then, to investigate the role of the WAVE complex, Hep2β cells were individually depleted using small interfering RNAs (siRNA) for Abi1, Sra1, Wave2 and Brk1, four members of this pentameric complex (Gautreau *et al*, 2004) (Fig 3A–D, Supplementary Fig S5). We simultaneously followed the uptake of IL-2Rβ and transferrin (Tf) by incubating cells with a fluorescent antibody against IL-2Rβ and fluorescent Tf for 15 min at 37°C (Grassart *et al*, 2008) (Fig 3A, B and D). We observed that depletion of Abi1, Wave2, Brk1 or Sra1 clearly inhibited IL-2Rβ entry (Fig 3A, B and D). Quantification of the data using Icy software (de Chaumont *et al*, 2012; Basquin *et al*, 2013) showed that the depletion of each member of the WAVE complex led to an inhibition of IL-2Rβ entry up to 65% (Fig 3D, Supplementary Fig S5A). Since the depletion of one subunit destabilizes the whole complex (Dubielecka *et al*, 2011), our results clearly show the involvement of the WAVE complex in IL-2Rβ uptake. In contrast, Tf uptake, requiring the clathrin-dependent route, was not affected (Fig 3A, B and D, Supplementary Fig S5B). Altogether, these data demonstrate that the WAVE complex is a new specific factor

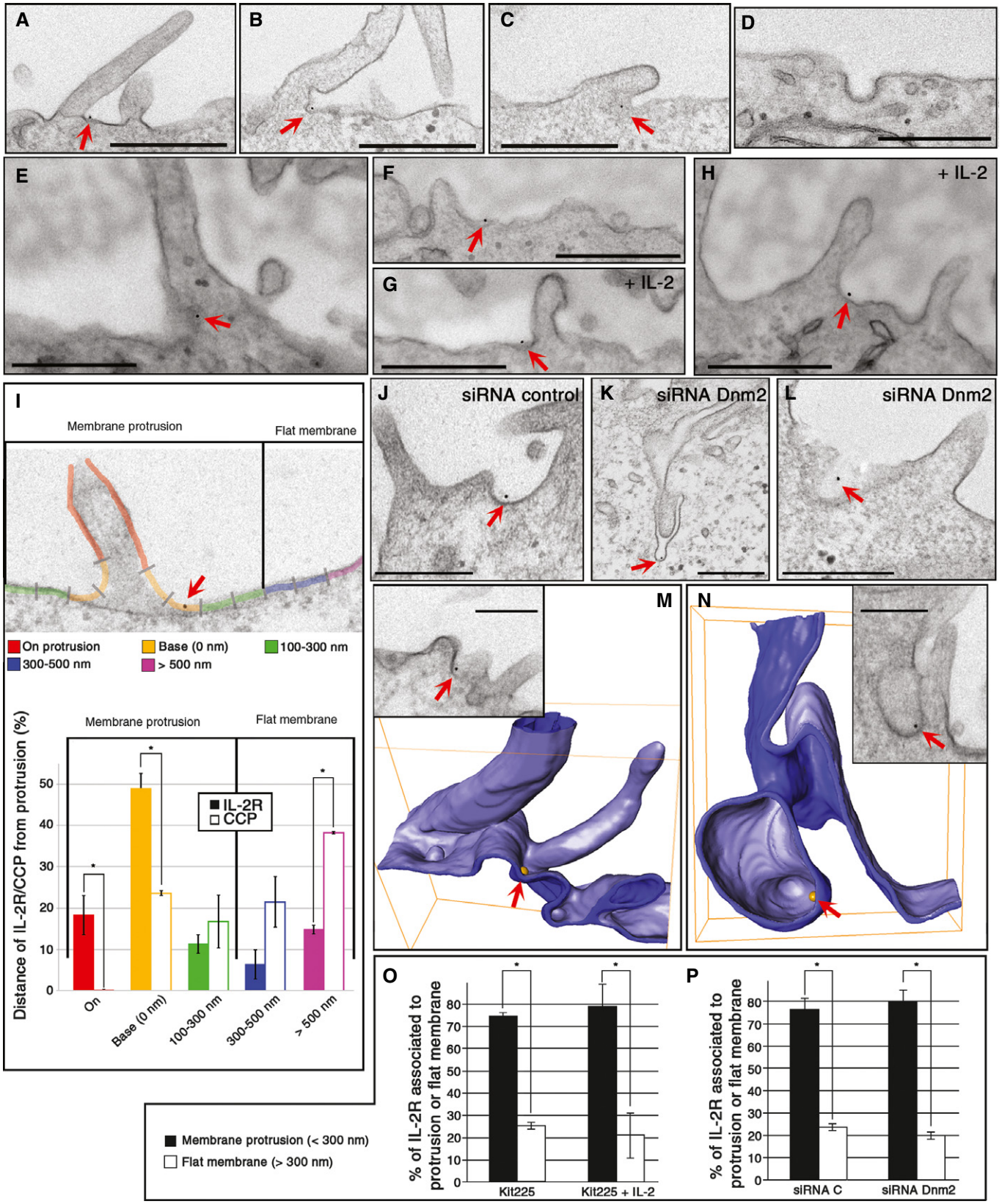

Figure 2.

Figure 2. IL-2R-containing pit is localized at the base of membrane protrusions.

A–P Hep2β cells depleted for dynamin 2 (siRNA Dnm2.1, K, L, P) or not (A–D, I, J, M, N) were incubated as described in Fig 1, and endocytosis was enabled by incubating the cells for 7 min at 37°C. Kit225 cells (E–H, O) were treated like Hep2β cells except that endocytosis was performed for 2 min at 37°C in the presence (G, H) or in the absence of IL-2 (E, F). Cells were fixed and embedded in epoxy resin, and sections were analysed by TEM (A–L, O, P) or electron tomography (M, N). (I) Distribution, in Hep2β cells, of plasma membrane IL-2R and clathrin-coated pits (CCP) with respect to the distance of the closest protrusion. All visualized gold beads or CCP were acquired in four different experiments (number of beads > 200), and distances to the nearest protrusion base were quantified using ImageJ (mean ± SE, unpaired *t*-test, $*P < 0.05$). (M, N) Electron tomographic models revealed IL-2R localization in small invagination (M, see also Supplementary Movie S1) and inside a large vesicle (N, see also Supplementary Movie S2). Arrows show IL-2R in pits at the plasma membrane. (O, P) Distribution of IL-2Rβ in two locations at the plasma membrane, associated with protrusions (< 300 nm) or with flat membrane (> 300 nm), in Kit225 cells with IL-2 or without IL-2 (O) or in Hep2β cells depleted or not for dynamin2 (P). IL-2R associated with protrusions (< 300 nm) or with flat membrane (> 300 nm) for each condition (mean ± SE, paired *t*-test, $*P < 0.05$). Scale bars represent 500 nm except for (M, N), 200 nm.

involved in the clathrin- and caveolae-independent internalization of IL-2Rβ.

Next, we tested the role of the WAVE complex in the recruitment of IL-2Rβ to membrane protrusions. After siRNA treatment, depleting the cells for Abi1 (Western blot in Supplementary Fig S3A), IL-2Rβ was immunogold labelled and TEM data were quantified as described in Fig 2. Strikingly, the depletion of Abi1 resulted in a strong reduction in the association of IL-2Rβ with protrusions compared to control cells (Fig 3E–I). Indeed, in Abi1-depleted cells, we found only 40% of IL-2Rβ in close proximity to protrusions compared to 80% in control cells (Fig 3E and I). Noteworthy, the amount of protrusions in Abi1-depleted cells was slightly affected (< 20%) compared to control cells (Supplementary Fig S4B and C), as was previously reviewed (Krause & Gautreau, 2014). This indicates that WAVE is required to drive the receptors to protrusions and/or is only involved in the formation of such protrusions. Nevertheless, these data point out the essential role of the WAVE complex in directing IL-2Rβ close to protrusions where the pit is created.

The WAVE complex interacts with IL-2R

To determine the role of the WAVE complex in bringing IL-2R to protrusions, we tested whether or not these two proteins interact. To do so, we constructed GFP-tagged forms of Wave2, Brk1 and Abi1, transfected them independently into Hep2β cells and immunoprecipitated them using antibodies directed against GFP. All three members of the complex could be co-immunoprecipitated with the other members of the complex, such as Sra1 (Fig 4). Strikingly, IL-2Rβ could also be co-immunoprecipitated with Brk1, Abi1 and Wave2 (Fig 4A and B, Supplementary Fig S6), in contrast to transferrin receptor, TfR (Fig 4B, Supplementary Fig S6). In addition, the depletion of Wave2 abrogates the co-immunoprecipitation between IL-2Rβ and Brk1, confirming the importance of the whole pentameric WAVE complex for this interaction (Fig 4B, Supplementary Fig S6). Altogether, these results confirm the specific interaction between IL-2R and the WAVE complex. Recent work by Chen *et al* (Chen *et al*, 2014) identified a consensus peptide motif, WIRS, which binds to a conserved site on the surface of the WAVE complex, formed by the Abi and Sra subunits. This motif is found in the intracellular tails of a large number of diverse neuronal receptors (Chen *et al*, 2014). Based on the definition of the WIRS consensus motif, Φ-x-T/S-F-x-x (Φ = preference for bulky hydrophobic residues; x = any residue), we found that the IL-2Rβ cytoplasmic tail contains a potential WIRS (peptide sequence YCTFPS) that is conserved throughout mammals, with the exception of rodents (see Fig 4C). To understand the role of this motif, we generated a mutant replacing the two conserved residues of the WIRS sequence (YCAAPS, called TFAA) and stably transfected it into Hep2 cells (Fig 4D and E). We found that mutating the WIRS motif impairs the binding of IL-2Rβ to the WAVE complex (Fig 4E) and affects its endocytosis (Fig 4D). Together, these data strongly indicate that IL-2Rβ contains a WIRS motif, which allows it to interact with the WAVE complex, a process essential for its internalization.

The WAVE complex and N-WASP are recruited at two stages of IL-2R uptake

Interestingly, our present and past (Grassart *et al*, 2010) results demonstrate that IL-2Rβ endocytosis requires two activators of Arp2/3-mediated actin polymerization: the WAVE complex (Fig 3) and N-WASP (Grassart *et al*, 2010). This new finding raises an important issue about the role of each activator and the step of endocytosis in which they are involved. The activators may act cooperatively or independently. Therefore, we analysed the time of recruitment of the WAVE complex, N-WASP and Arp2/3 during IL-2Rβ endocytosis using time-lapse total internal reflection fluorescence (TIRF) microscopy. This technique is very convenient to visualize events occurring close to the plasma membrane, including endocytosis and membrane protrusions (Merrifield *et al*, 2002; Xu *et al*, 2009). To allow the visualization of IL-2R endocytosis, the receptor was surface labelled (2 min at 37°C) with an anti-IL-2Rβ antibody coupled to Cy3 fluorochrome, the unbound antibodies were washed away, and then, cells were imaged with TIRF microscope for maximum 30 min at 37°C at 0.5 Hz. This allowed us to examine endocytosis and not exocytosis, since we observed only the internalization of the surface-labelled receptor (Hémar *et al*, 1995). At the plasma membrane, IL-2Rβ moved on the surface of the cell and some receptors stop, remaining stable and visible for approximately 110 s and finally disappearing from the TIRF field at the end of the endocytic process (Supplementary Movie S3, Fig 5A–F). We performed an automated analysis of TIRF images with the open-source image analysis software Icy (de Chaumont *et al*, 2012) to analyse at least 1,000 IL-2R tracks. This analysis allowed us to detect the tracks, co-localize them and sort out the intensity profile of each track. To observe the recruitment of the WAVE complex, Hep2β cells were transfected with GFP-Abi1 or GFP-Brk1 (Supplementary Fig S7), and TIRF analysis enabled the identification of IL-2R-WAVE co-localized tracks. We found that the WAVE complex appeared before IL-2Rβ clusters at the plasma membrane and disappeared before the entry of the receptor into the cell (Fig 5A and B). Quantitation of the data demonstrated that the WAVE complex (GFP-Abi1 and GFP-Brk1) appeared around 35 s before IL-2R, but

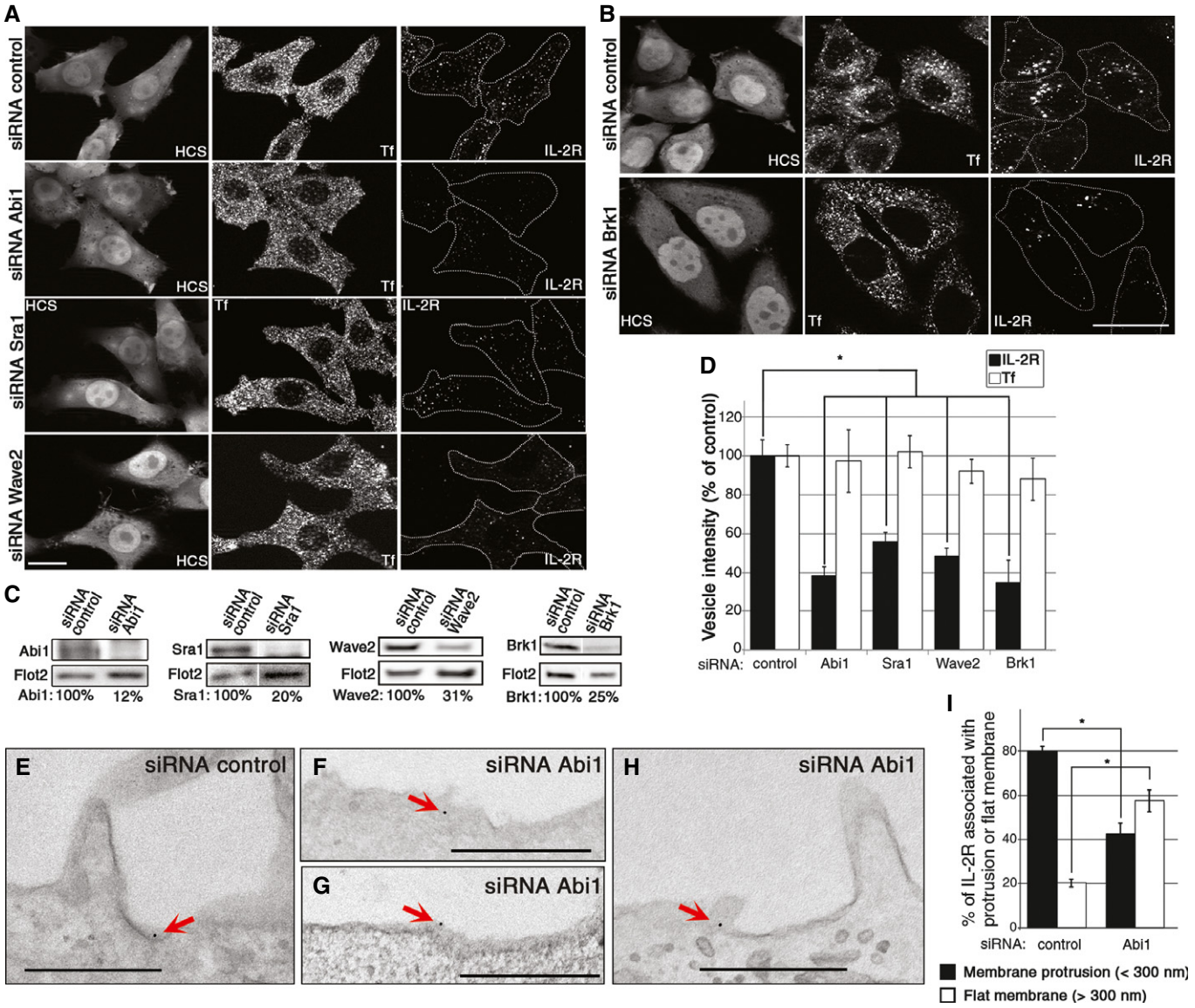

Figure 3. The WAVE complex drives IL-2R close to protrusions during endocytosis.

A, B Hep2β cells were transfected with siRNA against Abi1 (siRNA Abi1.1), Sra1 (siRNA Sra1.1), Wave2 (siRNA Wave2.1) and Brk1 (siRNA Brk1.1) or with a control siRNA (siRNA control). Endocytosis was observed by incubating cells with Tf coupled to AlexaFluor 488 (Tf) and with an anti-IL-2Rβ antibody coupled to Cy3 (IL-2R) for 15 min at 37°C. Cells were fixed and stained with HCS Cell Mask to detect cell boundaries. A medial section is shown. Scale bars: 10 μm.

C Western blots of siRNA-transfected cell lysates were probed using antibodies against Abi1, Sra1, Wave2 or Brk1 and against flotillin2 (Flot2) as a loading control. Quantification of proteins was performed with ImageJ using Flot2 to normalize the amount of loaded proteins. Results are expressed as a percentage of the control condition (siRNA control).

D Quantification of endocytosis from cells transfected with siRNAs (mean of two different siRNAs) was performed by measuring the number and fluorescence intensity of vesicles (vesicle intensity) per cell using Icy (mean ± SE; $n > 100$ cells in at least three independent experiments, unpaired t-test, $^*P < 0.05$). The results are expressed as percentage of the control cells.

E–I Hep2β cells were transfected with siRNA directed against Abi1 (siRNA Abi1.1, F–I), or a control siRNA (E), were incubated at 4°C with an anti-IL-2R antibody, then with protein A coupled to 10-nm gold beads and then incubated 7 min at 37°C. Cells were fixed and embedded in epoxy resin, and sections were analysed by TEM. (I) Quantification of TEM data as in Fig 2O and P showing the percentage of IL-2R associated with protrusions (< 300 nm, black bars) or with flat membranes (> 300 nm, white bars) for each condition (mean of triplicates ± SE, unpaired t-test, $^*P < 0.05$). Scale bar represents 500 nm. Arrows show IL-2R at the plasma membrane.

disappeared 40 s before the departure of the receptor (Fig 5G and H, Supplementary Fig S7C and E). These data show an early involvement of the WAVE complex during IL-2Rβ endocytosis. Then, we observed simultaneously IL-2Rβ and GFP-N-WASP (Fig 5C, D, G and H). In contrast to the WAVE complex, we observed that N-WASP was recruited subsequent to IL-2Rβ clustering at the plasma membrane (Fig 5C and D). Indeed, quantitative analysis showed N-WASP recruitment 30 s after IL-2R, and N-WASP remained close to the plasma membrane for 10 s after IL-2R disappearance (Fig 5G and H). Then, we observed simultaneously in

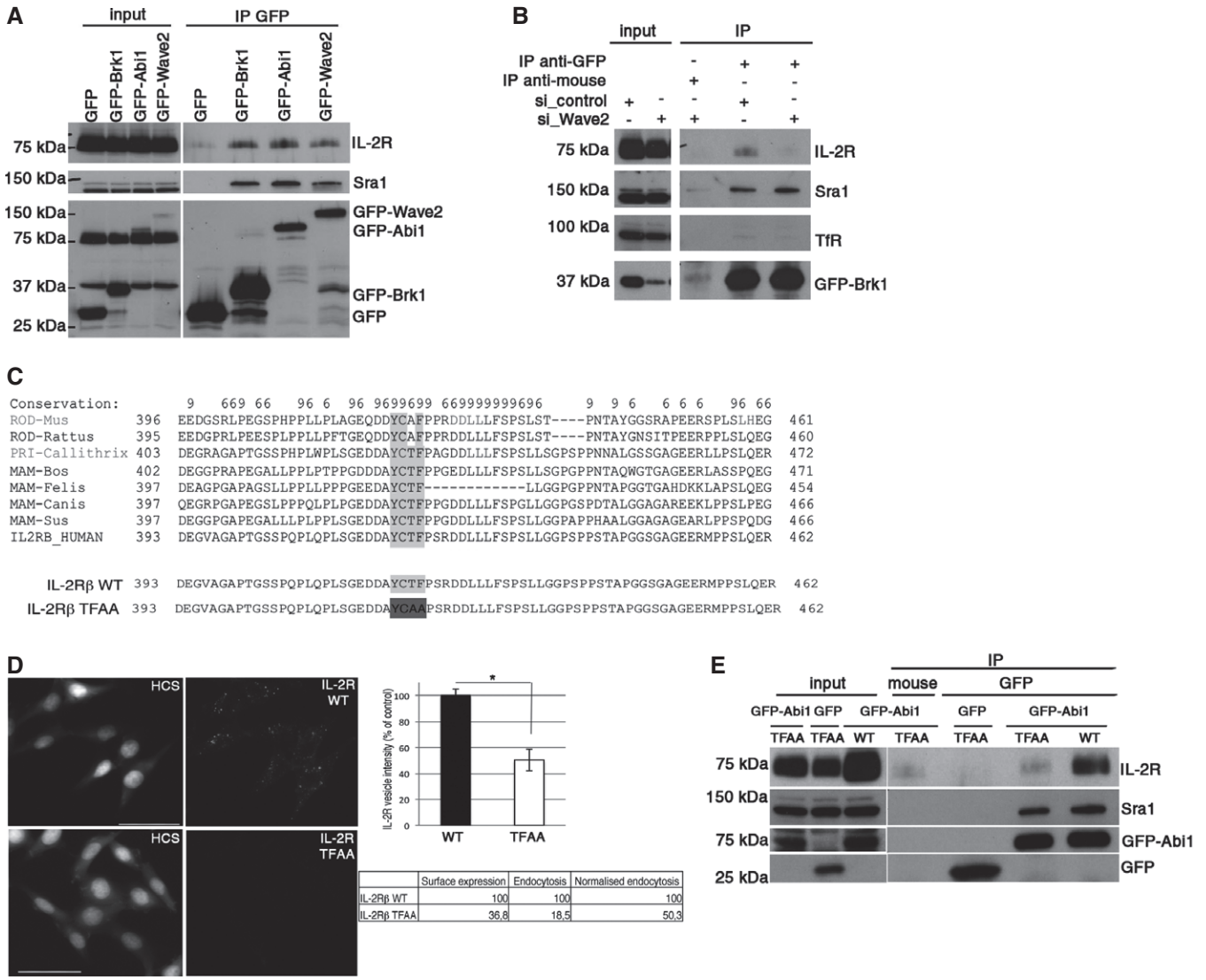

Figure 4. The WAVE complex interacts with IL-2R.

A Lysates of Hep2β cells transfected with GFP-Wave2, GFP-Abi1, GFP-Brk1 or GFP as a control were immunoprecipitated using an anti-GFP antibody. Western blots were probed using antibodies against IL-2R, GFP and Sra1, as a control of the WAVE complex co-immunoprecipitation.

B Hep2β cells were transfected with a siRNA targeting Wave2 (siRNA Wave2.2) or a control siRNA and then transfected 48 h later with GFP-Brk1. Co-immunoprecipitation using either GFP or mouse IgG antibody, Western blots were performed as described in (A). In addition, Western blots were labelled with antibody against TfR as a negative control of co-IP.

C Amino acid sequence alignment of IL-2Rβ homologues. Dark shaded sequences are identical and conserved and represent a putative WIRS sequence. Amino acid alignment of IL-2Rβ WT and the mutant in the WIRS named TFAA.

D Endocytosis was observed in Hep2β WT- and TFAA-mutant cells by incubating cells with an anti-IL-2Rβ antibody coupled to Cy3 (IL-2R) for 15 min at 37°C and triplicates were quantified as in Fig 3. Scale bars represent 20 μm. *$P < 0.05$.

E Lysates of Hep2β WT- and TFAA-mutant cells transfected with GFP-Abi1 or GFP were immunoprecipitated using an anti-GFP or anti-mouse IgG as described in (B).

TIRF GFP-p16, a subunit of Arp2/3, with IL-2Rβ (Fig 5E–H). Consistently, this experiment showed that Arp2/3 is recruited during two stages of endocytosis (Fig 5E and F). First, Arp2/3 appeared before the IL-2Rβ cluster, as for the WAVE complex, and remained visible after the entry of the receptor with a second peak of recruitment at the end of the process, like N-WASP (Fig 5E–H). Therefore, our results reveal two bursts of actin polymerization during IL-2Rβ uptake induced by the recruitment of two activators of Arp2/3 (WAVE, N-WASP) at two stages of the process (Fig 5G).

Dynamin 2 is a transition controller for WAVE/N-WASP recruitment

Considerable evidence supports the view that dynamin and actin filaments play interdependent roles during clathrin-dependent and clathrin-independent endocytic processes in mammalian cells (Menon & Schafer, 2013). Thus, we decided to analyse the role of dynamin in IL-2R endocytosis with respect to the two newly involved F-actin regulators: WAVE and N-WASP.

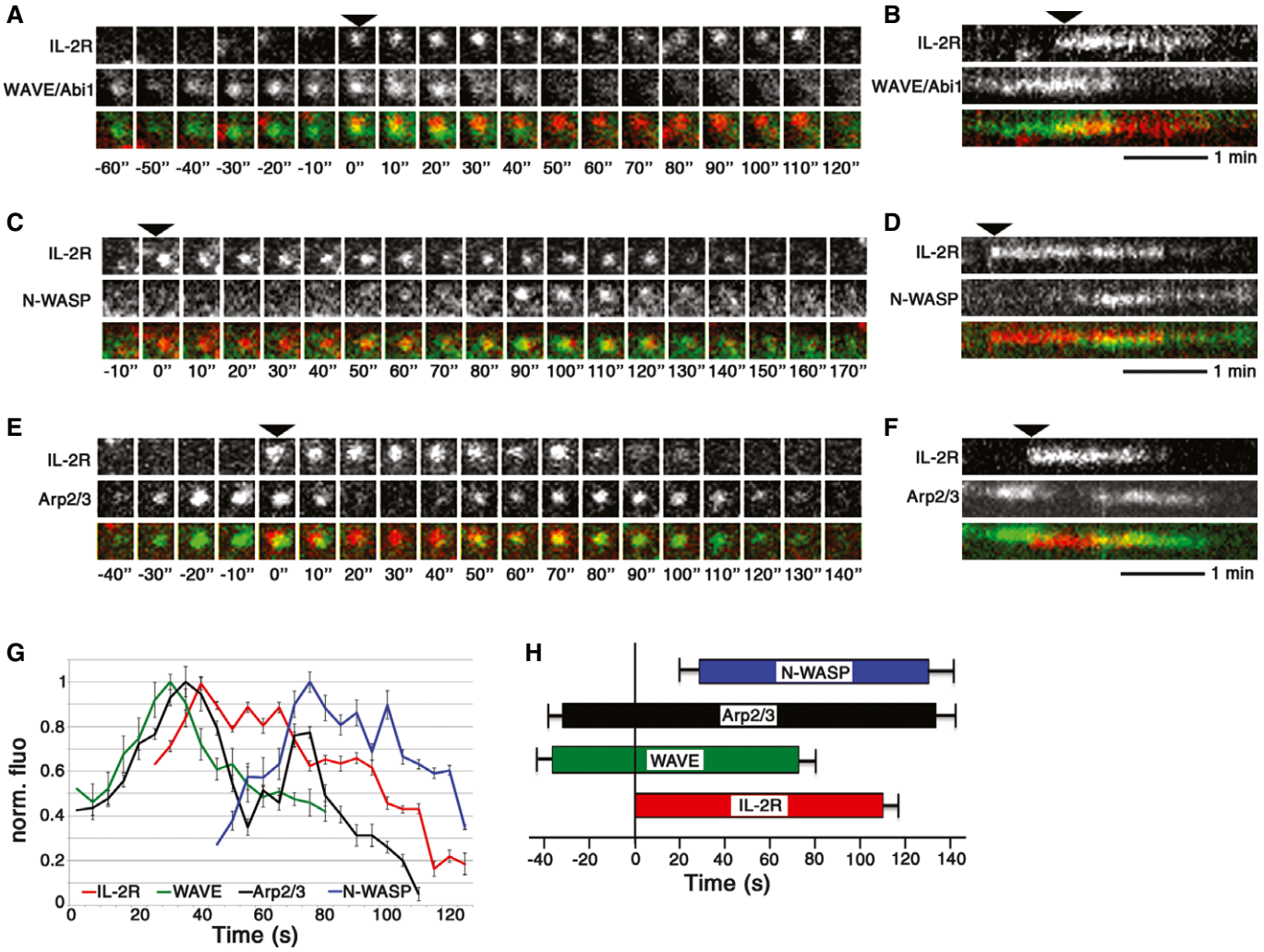

Figure 5. The WAVE complex and N-WASP are recruited at two stages of IL-2R endocytosis.

A–F TIRF images of Hep2β cells transfected with GFP-Abi1 representing the WAVE complex (A, B), GFP-N-WASP (C, D) or GFP-p16, a member of the Arp2/3 complex (E, F), and incubated with anti-IL-2Rβ-Cy3 antibody were obtained from a movie at 0.5 Hz. Representative kymographs of the events upon time are present in (B, D, F). Arrows indicate the appearance of IL-2Rβ clusters.

G, H Automated analysis of TIRF images with Icy software was done on 10 cells, analysing around 1,000 IL-2R tracks per condition. (G) Average fluorescence intensity profiles of WAVE, N-WASP and Arp2/3 with respect to IL-2R tracks, using normalized fluorescence intensities for each track (time 0 is arbitrarily determined by the first protein recruited, mean of 10 tracks, ± SE). (H) Mean time of appearance/departure of WAVE, N-WASP and Arp2/3 co-localized to IL-2R tracks, time = 0 represents the initiation IL-2R track (mean ± SE based on the analysis of around 1,000 IL-2R tracks).

First, we tested if dynamin directly or indirectly controls the interaction of IL-2Rβ with the WAVE complex. Hep2β cells were depleted for dynamin 2 and transfected with GFP-Brk1 or GFP; immunoprecipitation experiments were performed as described in Fig 4 (Fig 6A). Compared with control cells, dynamin-depleted cells showed an increase in the amount of IL-2Rβ co-immunoprecipitated with Brk1 (1.4 fold, Fig 6A). Thus, in the absence of dynamin 2, WAVE-IL-2R interaction is stronger and/or longer. This suggests that the recruitment of dynamin 2 affects IL-2R-WAVE interaction. To strengthen this hypothesis, we inhibited dynamin GTPase activity using dynasore (Macia *et al*, 2006) or dyngo-4A (Harper *et al*, 2011) that should block the vesicle formation after dynamin recruitment (Macia *et al*, 2006; Grassart *et al*, 2014), leading to persistence of dynamin 2 at endocytic sites (Grassart *et al*, 2014). In contrast to the depletion of dynamin 2, we observed that dynamin inhibition strongly decreased the co-immunoprecipitation of IL-2Rβ with the WAVE complex (> 80% reduction, Fig 6B). Thus, our data suggest that the prolonged presence of dynamin prevents the interaction between IL-2Rβ and the WAVE complex. These results are in total agreement with our TIRF analysis (Fig 5) and confirm the early involvement of the WAVE complex during IL-2Rβ pit and vesicle formation.

As off-target effects of dyngo-4A and dynasore have been reported previously, we decided to better investigate the role of dynamin during IL-2Rβ endocytosis. Thus, we performed TIRF live imaging in cells depleted for dynamin 2 and analysed WAVE,

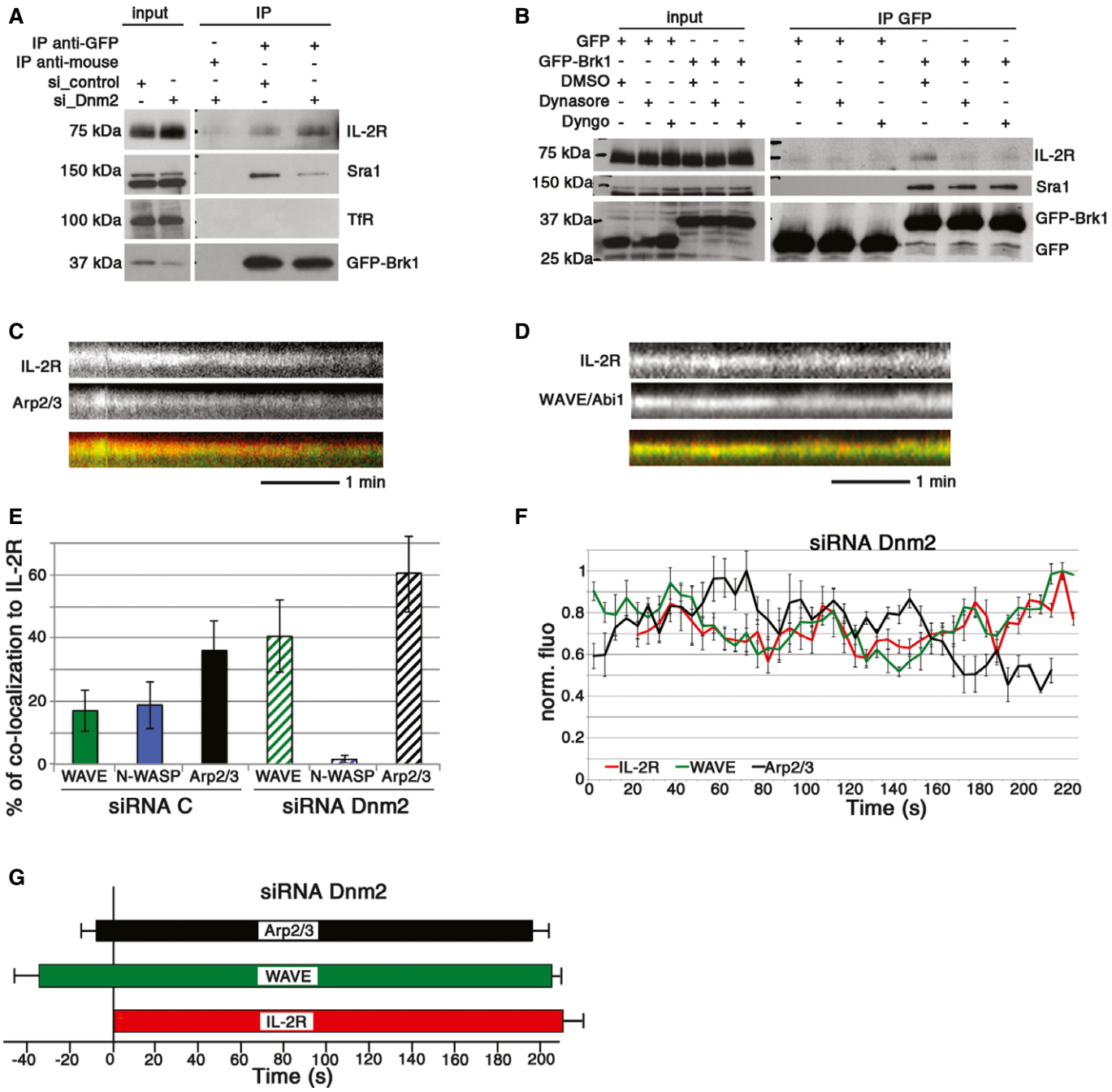

Figure 6. Dynamin 2 is a transition controller for WAVE/N-WASP recruitment.

A Hep2β cells were transfected with siRNA control or against dynamin 2 (siDnm2.2) and then transfected 48 h later with either GFP-Brk1 or GFP. Co-immunoprecipitation, Western blots were performed as described in Fig 4.

B Hep2β cells transfected with GFP-Brk1 or GFP were serum-starved and then incubated with 80 μM dynasore, 30 μM dyngo or DMSO as a control. Co-immunoprecipitation, Western blots were performed as described in Fig 4.

C–G Automated analysis of TIRF images of cells treated with siRNA control or siRNA Dnm2.1 using Icy software was done on 10 cells, analysing around 1,000 IL-2R tracks per condition. (C, D) Representative kymographs of Arp2/3-IL-2R track or of WAVE-IL-2R track. (E) Percentage of co-localized WAVE, N-WASP or Arp2/3 tracks to IL-2R. (F) Average fluorescence intensity profiles of WAVE and Arp2/3 with respect to IL-2R tracks using normalized fluorescence intensities for each track (time 0 is arbitrarily determined by the first track recruited, mean of 10 tracks, ± SE). (G) Mean time of appearance/departure of WAVE and Arp2/3 co-localized to IL-2R tracks, time = 0 represents the initiation IL-2R track (mean ± SE based on the analysis of around 1,000 IL-2R tracks).

N-WASP and Arp2/3 recruitment. As expected in dynamin 2-depleted cells, IL-2Rβ tracks were visible for longer periods of time in the TIRF field (i.e. at plasma membrane) than within control cells (compare Figs 6C, D, F and G and 5). This demonstrates the reliability of our TIRF methods to identify IL-2Rβ endocytic tracks and to study their dynamics. Strikingly, we did not see any co-localization

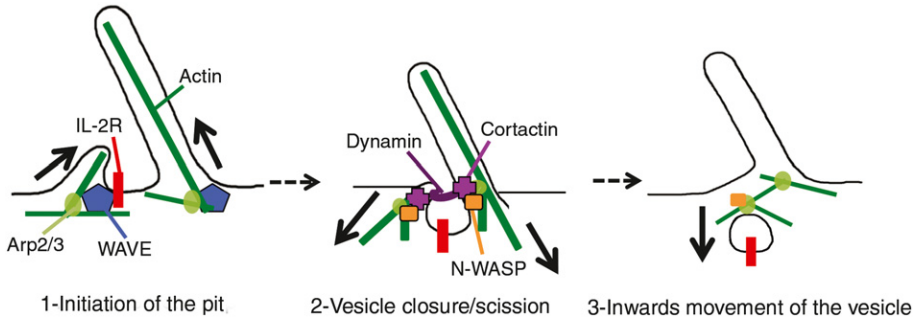

Figure 7. Protrusion-based endocytosis of IL-2R.
IL-2R by interacting with the WAVE complex is located at the basis of membrane protrusions, thereby creating an initial pit (1). This first step implicates outward forces (arrows) induced by the WAVE complex-mediated actin polymerization (1). Once the pit would be done, dynamin would be recruited to the neck of the vesicle and the scission of the vesicle would be helped by the cortactin, N-WASP and another round of branched actin polymerization (2). This second step involves inward forces (arrows) generated by N-WASP-mediated actin polymerization (2). Finally, the vesicle would migrate inside the cell, thanks to actin polymerization, and would eventually fuse to early endosome (3).

between IL-2Rβ and N-WASP at the plasma membrane (Fig 6E). In contrast, we found a two-fold increase in the amount of co-localized tracks between IL-2Rβ and either Abi1 (WAVE complex) or p16 (Arp2/3) (Fig 6E). Coherently, in the absence of dynamin 2, GFP-Abi1-IL-2R or GFP-Brk1-IL-2R, and GFP-p16-IL-2R tracks were co-localized much longer than in the control cells (compare Figs 6 and 5, Supplementary Fig S7). These TIRF data indicate that dynamin 2 controls the departure of the WAVE complex and is necessary for N-WASP recruitment to IL-2Rβ tracks at the plasma membrane. Altogether, these results reveal the pivotal and dual role played by dynamin 2 in the clathrin-independent endocytosis of IL-2Rβ. Indeed, our ultrastructural data confirm the involvement of this large GTPase in the scission of the IL-2Rβ vesicle. In addition, our immunoprecipitation and TIRF data reveal the second action of dynamin 2 as a transition controller for the recruitment of two Arp2/3 activators: WAVE and N-WASP.

Discussion

This study reveals a new mechanism that we call protrusion-based endocytosis, which is used to internalize receptors into small vesicle (Fig 7). So far, all models of receptor-mediated endocytosis begin with the invagination from the flat plasma membrane using coat component. For example, during clathrin-mediated endocytosis, the recruitment of proteins, such as the BAR domain FCHO, AP-2 and clathrin, are required for the induction of the first invagination of flat plasma membrane in order to form the pit (Reider *et al*, 2009; Henne *et al*, 2010; McMahon & Boucrot, 2011; Cocucci *et al*, 2012). Therefore, the current model for endocytic pit formation is the inward bending of the membrane directed by proteins/lipids inducing the invagination (Mooren *et al*, 2012). In this work, we show that IL-2R endocytosis requires its recruitment at the base of protrusions via its association with the WAVE complex. It does not seem that IL-2R induces protrusions, but rather that IL-2R, through interactions with the WAVE complex via its WIRS motif, would be recruited to these structures. The WAVE-induced, outward forces generating protrusions would create at its base the initial invagination to form the pit where IL-2Rβ would be trapped. This initial pit at the base of the WAVE complex would allow IL-2R to cluster. The formation of such an initial depression is not homogenous. This is consistent with the variation of vesicles sizes, whose morphology is not as calibrated as for clathrin- or caveolin-coated vesicles. Also, our results are clearly distinct from previous findings showing that clathrin-coated pits can close with the formation of a protrusion at one side of the pit (Shevchuk *et al*, 2012). In this previous report, the protrusion was solely involved in the scission of some of the CCPs. Instead, our present study indicates that protrusions initiate the creation of the clathrin-independent endocytic pit.

Interestingly, other cargos might use this protrusion-based endocytosis. One candidate might be the insulin receptor that was previously shown as strongly associated with villi at the cell surface of lymphocytes (Carpentier *et al*, 1981). A recent work described a clathrin-/caveolin-independent, though dynamin-/endophilin-dependent, pathway called FEME that is used by IL-2R, as well as several G-protein-coupled receptors, including α_{2a}- and β_1-adrenergic, dopaminergic D3 and D4 receptors, muscarinic acetylcholine receptor 4, and receptor tyrosine kinases like EGFR (Boucrot *et al*, 2015). Coherently with our study, this pathway is prominent at the leading edges of the cell that coincide with protrusive activity. Another list of putative cargos using protrusion-based endocytosis may include receptors having a WIRS motif allowing their interaction with the WAVE complex (Chen *et al*, 2014). Indeed, the Rosen laboratory has identified around 120 diverse membrane proteins, including protocadherins, ROBOs, netrin receptors, neuroligins, GPCRs and channels (Chen *et al*, 2014), all of which are potential candidates.

In addition, our study reveals the key role of Arp2/3-mediated actin polymerization during IL-2R endocytosis. Indeed, the Arp2/3 inhibitor, CK-666, strongly affects IL-2R (90% of inhibition, Supplementary Fig S4); in contrast, the clathrin-dependent pathway was less affected (50% of inhibition, Supplementary Fig S4). The fact that two Arp2/3 activators, N-WASP and the WAVE complex, are involved in IL-2R endocytosis, whereas only N-WASP is required for clathrin-dependent endocytosis, might account for this difference. Indeed, in the case of IL-2R endocytosis, we observed two bursts of actin polymerization. The first burst mediated by the WAVE complex appears before IL-2Rβ clustering; it should be responsible for the recruitment of the receptor at the endocytic site to initiate pit formation. Then, N-WASP induces a second round of

Arp2/3-mediated actin polymerization at a later stage just before the internalization of IL-2Rβ. This last event of actin polymerization should aid inward forces of the new-born vesicle to detach from plasma membrane and to enter deeper inside into the cell, as it is proposed for the clathrin-dependent pathway (Boulant *et al*, 2011; Taylor *et al*, 2011). Therefore, our work identifies the unique feature of clathrin- and caveolae-independent internalization of IL-2Rβ that requires two rounds of actin polymerization induced by two activators and triggers two stages of the process, pit initiation and vesicle scission.

Another important finding of our work concerns the dual role of dynamin in the clathrin-independent process. Thanks to our ultrastructural data showing the abnormal IL-2Rβ pit morphology in the absence of dynamin, our work reinforces the role of this GTPase in the vesicle scission. The second role of dynamin would be a transition controller for the recruitment of actin regulators during IL-2R endocytosis. Indeed, our dynamic analysis reveals that dynamin is required for the recruitment of N-WASP during the last step of endocytosis. This recruitment of N-WASP promotes F-actin that would generate inward forces to detach the vesicle from the plasma membrane in combination with the pinchase activity of dynamin. Indeed, previous studies have shown that many dynamin-interacting partners, like cortactin, link dynamin to actin polymerization via Arp2/3 complex and N-WASP (Menon & Schafer, 2013). In the case of IL-2R uptake, cortactin–N-WASP interaction was shown to be essential (Grassart *et al*, 2010). Thus, our work, as well as past data, indicates that the recruitment of dynamin will bring together cortactin, N-WASP and Arp2/3 complex to allow the scission of the IL-2R vesicle.

The remaining point to be discussed is the regulation of the recruitment of actors of IL-2Rβ endocytosis. We previously identified Rac1 and PI3K as specific and essential upstream regulators of IL-2R uptake (Basquin *et al*, 2013). We already proposed that they would allow the recruitment of N-WASP to cortactin, with cortactin itself being linked to dynamin (Gesbert *et al*, 2004; Grassart *et al*, 2008; Basquin *et al*, 2013). Therefore, Rac1 and PI3K should regulate the last step of endocytosis, the vesicle scission. However, our new result implicates the WAVE complex at a very early stage of IL-2Rβ uptake, modifying our view on the role of these regulators. Indeed, the WAVE complex is clearly known to be stimulated at the plasma membrane by the Rac GTPase and $PI(3,4,5)P_3$ (Lebensohn & Kirschner, 2009). Rac1 and PI3K could thus also promote the initiation of the IL-2Rβ-containing pits, acting as general regulators of several stages of the IL-2R endocytosis.

Materials and Methods

Cells, constructs, siRNA and reagents

Hep2β cells stably expressing IL-2Rβ (Grassart *et al*, 2008) were grown in DMEM containing 10% FCS and 1 mg/μl of geneticin (Gibco). The human T-cell line Kit225 was maintained in RPMI containing 10% FCS and 200 pM IL-2 (a gift from A. Minty, Sanofi-Synthélabo, Labege, France). The dynamin inhibitors dynasore (abcam) and Dyngo-4A^{TM} (abcam) were used at 80 μM and at 30 μM, respectively, and incubated with serum-starved cells for 45 min at 37°C. CK-666 (Arp2/3 inhibitor) or CK-689 (inactive inhibitor) both from MERCK CHEMICALS were used at 100 μM. Constructs used were GFP-N-WASP which was a generous gift from Dr. B. Qualmann (Kessels & Qualmann, 2002). GFP-Abi1, GFP-Brk1, GFP-Wave2 and GFP-p16 were obtained by subcloning Abi1, Brk1, Wave2 and p16 (Gautreau *et al*, 2004) into pcDNA-FR-PC-GFP vector. Small interfering RNA (siRNA) were synthesized by Thermo Scientific Dharmacon. Sense sequences were for siRNA CHC: TAATCCAATTCGAAGACCAAT (Sauvonnet *et al*, 2005), siRNA Abi1.1, 2: UAAUAGCACCUGCGAAUAU and GGACGGAAUACUCCU UAUA, siRNA Sra1.1, 2: GAUAAACGGUUACGAUCAG and GAGUAC GGCUCUCCUGGUA, siRNA Wave2.1, 2: GGAUUAGAUCAUUAGCUC ATT and GCAAAUGGUUGUAGUAAUU, siRNA Dnm2.1, 2: GCAG CUCAUCUUCUCAAAATT and GAGCGAAUCGUCACCACUU, siRNA Brk1.1, 2: GGGCUAACCGGGAGUACAU and GGAGAAUAGAGUA CAUUGA, and control siRNA was ON-TARGET plus control (Thermo Scientific Dharmacon). IL-2Rβ mutated on threonin 420 and phenylalanin 421 to alanin residues (TFAA) was obtained by PCR using the QuikChange site-directed mutagenesis kit (Stratagene) and the following oligonucleotide: 5′-GTCAGGGGAGGACGACGCCTACTGCG CCGCCCCCTCCAGGGATGACCTGCTGCTC-3′. All constructs were verified by sequence analysis, and one clone was stably transfected into Hep2 cells to create the HepβTFAA cell line.

Transfection

Plasmid introduction was done using electroporation (300 V and 500 F, Biorad) of 4×10^6 Hep2β cells with 4 μg of DNA for GFP and GFP-Brk1 or 10 μg for GFP-Abi1, GFP-Wave2, GFP-N-WASP and GFP-p16, and after 24 h, cells were used to monitor endocytosis or immunoprecipitation experiments. For siRNA transfection, 5 pmol (Figs 2 and 3) or 20 pmol (Figs 4 and 6, Supplementary Fig S7) of siRNA was introduced by using Lipofectamine^{TM} RNAiMAX (Invitrogen) in 0.5×10^5 Hep2β cells (Figs 2 and 3) or 1.5×10^6 Hep2β cells (Figs 4 and 6). All siRNA-transfected cells were analysed 72 h after transfection, whereas plasmid-transfected cells were analysed 48 h after transfection.

Endocytosis, immunofluorescence, FACS and microscopy

Hep2β were incubated with Tf coupled to AlexaFluor 488 (TfA488, Molecular Probes) and anti-IL-2Rβ (561) antibody coupled to cyanine 3 (Cy3) for a time course up to 15 min at 37°C to allow receptor entry (Grassart *et al*, 2010). This monoclonal antibody, 561, recognizes the extracellular part of IL-2Rβ and does not affect the binding of the ligand IL-2 nor the traffic of the receptor (Subtil *et al*, 1994). Cells were fixed and permeabilized as described in Grassart *et al* (2008). To detect cell boundaries, cells were stained with HCS Cell Mask Alexa Fluor 350 (Invitrogen Molecular Probes, 1.25 ng/ml). Fluorescence images were obtained with an Apotome fluorescent microscope (Zeiss) and a Roper Scientific Coolsnap HQ camera equipped with a 63× objective to acquire a Z series of 1-μm optical sections, a medial section was shown in the Figures. In parallel, to estimate the level of IL-2Rβ/TfR expression at the cell surface, we incubated cells with 561 coupled to AlexaFluor647 (Anti-IL-2RA647) and TfA488 at 4°C for 1 h, washed and analysed with a FACSCalibur flow cytometer (BD Biosciences). At least 5,000 cells were analysed in three different experiments. We normalized the surface expression in each condition to the control condition,

and these data were used to normalize our quantitative data of endocytosis (see details in Supplementary Fig S5). For endocytosis quantification, images were obtained with a 20× objective under the same acquisition settings. Images collected from at least three independent experiments, representing at least 100 cells, were further analysed and quantified using Icy software as described (Grassart *et al*, 2010; Basquin *et al*, 2013).

Immunoprecipitation and Western blotting

Hep2β or Hep2βTFAA cells (4×10^6) transfected with plasmids and/or siRNA or with plasmids and/or then drug-pre-treated were lysed on ice-cold buffer (50 mM Tris pH 7.4, 50 mM NaCl, 2 mM EDTA and 1% NP-40) and centrifuged for 20 min at 15,000 *g* at 4°C to obtain the lysates. Lysates were incubated with either anti-GFP mouse antibody (4E6) or anti-mouse IgG (Jackson ImmunoResearch), washed and mixed with protein A-Sepharose™ CL-4B (GE Healthcare), and bound proteins were eluted by boiling in Laemmli buffer for 5 min, loaded on SDS-PAGE and analysed by Western blot (WB). Antibodies (Ab) used for WBs were anti-Sra1, anti-Wave2 and anti-Abi1 rabbit Ab (Gautreau *et al*, 2004), anti-GFP rabbit Ab (Santa Cruz Biotechnology) (Santa Cruz Biotechnology), anti-IL-2Rβ rabbit Ab (Santa Cruz Biotechnology), anti-dynamin mouse Ab (Sigma Aldrich), anti-transferrin receptor mouse Ab clone H68.4 (Life technologies), anti-clathrin heavy chain mouse antibody (BD Transduction Laboratories) and anti-flotillin2 mouse Ab (BD Biosciences) for loading controls. Secondary antibodies used were the enzyme horseradish peroxidase (HRP) linked to anti-rabbit (GE Healthcare) and visualized by ECL, or alkaline phosphatase linked to anti-mouse, (Pierce) visualized by ECF and quantified by Storm FluoroImager. For all WBs, input represents 2.5% of total lysate loaded on the gel. For Western blot quantification, the total intensity of each band was quantified using ImageJ and background was subtracted. For Supplementary Fig S6, histograms represent the relative amount of IL-2R co-immunoprecipitated to GFP-tagged protein compared to control cells (considering 100% of Co-IP in GFP-Brk1-transfected control cells) and normalized using the level of Sra1 or GFP immunoprecipitated (mean made on three independent experiments ± SE, unpaired *t*-test).

TIRF microscopy

Hep2β cells (3×10^5), depleted or not for Dnm2 by siRNA treatment, were transfected with GFP-Abi, GFP-Brk1, GFP-N-WASP or GFP-p16 and plated on MatTek plates. Then, cells were labelled during 2 min at 37°C with anti-IL-2Rβ-Cy3 antibody in a TIRF medium (25 mM HEPES, 135 mM NaCl, 5 mM KCl, 1.8 mM $CaCl_2$, 0.4 mM $MgCl_2$, 4.5 g/l glucose and 0.5% BSA, pH 7.4) and washed. Then, we incubated cells in an environmental control system set to 37°C and we imaged movies of 600 s at 0.5 Hz. Experiments were performed using a TIRF microscope (IX81F-3, Olympus) having a 100× NA 1.45 Plan Apo TIRFM Objective (Olympus) and controlled by CellM (Olympus). Two solid-state laser lines (561 and 488 nm) (Olympus) were coupled to a TIRF condenser through two optical fibres. We acquired simultaneously the two colour channels through a Dual View beam splitter (Optical Insights), which separates the two emission signals, with a dichroic mirror and emission filters (Basquin *et al*, 2013). Images were collected using an IxonEM+ camera (DU885, Andor). Analysis of TIRF movies (10 per condition, five movies for Supplementary Fig S7) was performed using Icy software.

Image analysis

We performed the automated analysis of TIRF images with the open-source image analysis software Icy (de Chaumont *et al*, 2012) (http://icy.bioimageanalysis.org).

Automatic detection of fluorescent spots

We detected automatically the molecule fluorescent spots that are significantly brighter than the cell background with a wavelet-based detection algorithm implemented as a plugin (Spot Detector plugin) in Icy.

Molecule tracking

Due to the high density of molecule spots and the low signal to noise ratio leading to missing and false detections, standard Bayesian tracking algorithms fail to track robustly the different endocytic molecules. We thus developed a new tracking algorithm that exploits the confinement of endocytic molecules at the cell membrane during the IL-2R endocytosis. In this algorithm, we first detect automatically the bright fluorescent molecule spots at each acquisition time (see above). We then stack the obtained detections and determine the positions of the putative endocytic events in the stacked image by detecting the very bright spots (intensity > 40 × (spot mean intensity)). Indeed, we expect that molecules appear many times at these endocytic positions as they interact with IL-2R during endocytosis. Conversely, molecules that are not confined and that diffuse freely at the cell membrane will not generate very bright spots in stacked image. Once we have obtained the positions of the putative endocytic events, we then reconstruct the endocytic tracks with a backtracking procedure: we associate the different detections to the nearest endocytic positions. To avoid the association of diffusing molecules with the endocytic tracks, we set a maximal association distance of 10 pixels. In addition, when two detections can be potentially associated with the same track, we choose the closest. As different endocytic events can happen at the same position, we set a maximal time gap of 20 s (10 frames) between two consecutive detections. Otherwise, we create two successive endocytic tracks at the same position. Our tracking algorithm is publicly available as an Icy plugin (eTrack plugin). In total for each condition, 10 cells were imaged generating 10 movies and for each, between 100 and 150 IL-2R tracks were obtained and analysed for co-localization (at least 1,000 IL-2R tracks analysed per condition).

Co-localization analysis of tracks

The analysis was done on at least 1,000 IL-2R tracks per condition. First, we filtered shortest tracks (< 4 s for all molecules or < 40 s for IL-2R), and we determined co-localized tracks if at some time the centre of mass of the two tracks is inferior to 4 pixels. This led us to obtain the percentage of co-localized tracks of GFP-Abi1 (WAVE), GFP-N-WASP or GFP-16 (Arp2/3) with IL-2R tracks (Fig 6E). In addition, we determined the time of recruitment of each track with respect to its co-localized IL-2R-track and measured the duration of co-localization (Figs 5H and 6G, Supplementary Fig S7E

and F). Finally, we quantified the fluorescence five frames before and five frames after the appearance/departure of each track, normalized the data upon max intensity of each track and exported into Excel file to draw the curve of intensities for WAVE, N-WASP, Arp2/3 and IL-2R. We compared IL-2R tracks of similar duration with the mean fluorescence intensity profiles of WAVE, N-WASP and Arp2/3, time 0 being arbitrarily determined by the first protein recruited (for Figs 5G and 6F mean of 10 tracks, for Supplementary Fig S7C and D mean of 5 tracks, ± SE).

Cell preparation for electron microscopy analysis

Hep2β or Kit225 cells incubated on ice with DMEM containing 10% FCS and 0.2% BSA for 20 min. To label IL-2Rβ, an antibody recognizing the extracellular part of the receptor (561 (Subtil *et al*, 1994)) was added for 20 min at 4°C and washed and cells were incubated with protein A coupled to 10-nm gold beads at 4°C (dilution 1/25, Aurion), washed and further incubated for 7 or 12 min (for Hep2β) and for 2 or 7 min (for KitT225) at 37°C to allow endocytosis. To label transferrin (Tf), Tf-10-nm gold conjugate (dilutions 1/50 or 1/100, Cytodiagnostics) was incubated with the cells at 4°C for 20 min, washed and further incubated at 37°C for 7 min. Cells were then fixed in 2% glutaraldehyde (Agar) diluted in 0.1 M sodium cacodylate buffer at pH 7.4 (EMS). Cells were washed on ice with the same buffer and incubated for 1 h in 1% osmium tetroxide (EMS) reduced with 1.5% potassium ferrocyanide (Karnovsky, 1971) diluted in 0.1 M sodium cacodylate. Cells were dehydrated on ice through graded concentration of ethanol (50–70–96–100%) and infiltrated in epoxy resin (Agar 100 resin kit, Agar) at room temperature according to the manufacturer's instructions and polymerized for 48 h at 60°C. Kit225 cells were processed identically, except that cells were concentrated by pre-embedding them prior to dehydration with low melting-point agarose (Promega).

Transmission electron microscopy (TEM)

Ultrathin sections (70 nm) were cut with an ultramicrotome (Ultracut, Leica Microsystems) and collected on 200-mesh copper grids (Agar). For sectioning of adherent Hep2β cells, their flat embedding allowed the collection of cell slices from the basal side and up to the first 800 nm from the coverslip. Sections were then stained with 2.5% aqueous uranyl acetate (Prolabo) and 1% lead citrate (Agar) before observation with a Zeiss 912 Omega TEM, JEM 1400 (Jeol) or Tecnai 12 (FEI corp.) microscope operation at 80 kV. Zeiss and Tecnai12 as well as JEM 1400 were equipped with side-mounted 2k × 2k Veleta (Olympus) and bottom-mounted Orius (SC1000, Gatan Inc.) CCD cameras, respectively, and controlled with iTEM (Olympus) or Digital Micrograph (Gatan) softwares and subsequently processed with ImageJ, considering that IL-2Rβ or CCP is close to a protrusion if distance is < 300 nm. CCPs were identified visually by the presence of the electron-dense coating of the membrane having a regular structure of about 100 nm in diameter.

To quantify cell protrusion, micrographs of individual cells were acquired at low magnification. Protrusions were counted, and the ratio of protrusion number to membrane length was calculated and compared to control cells (n = 30).

Electron tomography

For electron tomographic analysis, two consecutive 150-nm-thick sections were cut from trimmed Epon block that was prepared as for TEM analysis. Images were acquired with Tecnai FEG 20 (FEI corp.) operating at 200 kV equipped with 4k × 4k Ultrascan 4000 CCD camera (Gatan Inc.) using SerialEM software (http://bio3d.colorado.edu/SerialEM/). Tilt series were collected over a tilt range of ± 62° with one-degree interval at nominal magnification of 14,500× providing a 2× binned pixel size of 1.53 nm. Gold particles of 10 nm in size were placed on top/below the sections to serve as fiducial markers; however, all gold particles were erased from the images to reduce the artefacts cast by these markers in the reconstructions. The dual-axis tomograms were reconstructed using IMOD software package (http://bio3d.colorado.edu/imod) prior segmentation, modelling and visualization with Amira software (FEI corp.).

Supplementary information for this article is available online: http://emboj.embopress.org

Acknowledgements

We thank Dr. P. Dehoux for his help on sequence analysis. In addition, we warmly thank Drs A. Danckaert and N. Aulner and the Plate-Forme d'Imagerie Dynamique of Institut Pasteur. We also like to thank Dr A. Grassart, Dr B. Qualmann and Pr. A. Dautry-Varsat and Pr. P. Sansonetti. Mervi Lindman and Maiju Saarekas from Univ. of Helsinki are thanked for technical assistance. In addition, we thank Mrs V. Demanoff and Dr. E.T. Arena for English correction. CB was supported by ED n°426 "Gènes, Génomes, Cellules" fellowship and by "la Ligue Nationale Contre le Cancer". This project was partly funded by the PTR387.

Author contributions

CB performed most of the experiments and VM assisted him. MT, HV and EJ performed electron microscopy studies. LR assisted with co-immunoprecipitation experiments. TL and JCOM designed plugins for Icy software to analyse TIRF data. AG provided several WAVE constructs. NS performed TIRF experiments, analysed the data and designed the study.

Conflict of interest

The authors declare that they have no conflict of interest.

References

Basquin C, Malarde V, Mellor P, Anderson DH, Meas-Yedid V, Olivo-Marin JC, Dautry-Varsat A, Sauvonnet N (2013) The signalling factor PI 3-kinase is a specific regulator of the clathrin-independent dynamin-dependent endocytosis of IL-2 receptors. *J Cell Sci* 126: 1099 – 1108

Basquin C, Sauvonnet N (2013) Phosphoinositide 3-kinase at the crossroad between endocytosis and signaling of cytokine receptors. *Commun Integr Biol* 6: e24243

Boucrot E, Ferreira AP, Almeida-Souza L, Debard S, Vallis Y, Howard G, Bertot L, Sauvonnet N, McMahon HT (2015) Endophilin marks and controls a clathrin-independent endocytic pathway. *Nature* 517: 460 – 465

Boulant S, Kural C, Zeeh JC, Ubelmann F, Kirchhausen T (2011) Actin dynamics counteract membrane tension during clathrin-mediated endocytosis. *Nat Cell Biol* 13: 1124 – 1131

Carpentier JL, Van Obberghen E, Gorden P, Orci L (1981) Surface redistribution of 125I-insulin in cultured human lymphocytes. *J Cell Biol* 91: 17 – 25

de Chaumont F, Dallongeville S, Chenouard N, Herve N, Pop S, Provoost T, Meas-Yedid V, Pankajakshan P, Lecomte T, Le Montagner Y, Lagache T, Dufour A, Olivo-Marin JC (2012) Icy: an open bioimage informatics platform for extended reproducible research. *Nat Methods* 9: 690 – 696

Chen B, Brinkmann K, Chen Z, Pak CW, Liao Y, Shi S, Henry L, Grishin NV, Bogdan S, Rosen MK (2014) The WAVE regulatory complex links diverse receptors to the actin cytoskeleton. *Cell* 156: 195 – 207

Cocucci E, Aguet F, Boulant S, Kirchhausen T (2012) The first five-seconds in the life of a clathrin-coated pit. *Cell* 150: 495 – 507

Damke H, Baba T, Warnock DE, Schmid SL (1994) Induction of mutant dynamin specifically blocks endocytic coated vesicle formation. *J Cell Biol* 127: 915 – 934

Dubielecka PM, Ladwein KI, Xiong X, Migeotte I, Chorzalska A, Anderson KV, Sawicki JA, Rottner K, Stradal TE, Kotula L (2011) Essential role for Abi1 in embryonic survival and WAVE2 complex integrity. *Proc Natl Acad Sci USA* 108: 7022 – 7027

Gaffen SL (2001) Signaling domains of the interleukin 2 receptor. *Cytokine* 14: 63 – 77

Gautreau A, Ho HY, Li J, Steen H, Gygi SP, Kirschner MW (2004) Purification and architecture of the ubiquitous Wave complex. *Proc Natl Acad Sci USA* 101: 4379 – 4383

Gesbert F, Sauvonnet N, Dautry-Varsat A (2004) Clathrin-independent endocytosis and signalling of interleukin 2 receptors. In *CTMI Volume*, Madshus DHI (ed.), Vol. 286, pp 119 – 148. Berlin: Springer

Grassart A, Dujeancourt A, Lazarow PB, Dautry-Varsat A, Sauvonnet N (2008) Clathrin-independent endocytosis used by the IL-2 receptor is regulated by Rac1, Pak1 and Pak2. *EMBO Rep* 9: 356 – 362

Grassart A, Meas-Yedid V, Dufour A, Olivo-Marin JC, Dautry-Varsat A, Sauvonnet N (2010) Pak1 phosphorylation enhances cortactin-N-WASP interaction in clathrin-caveolin-independent endocytosis. *Traffic (Copenhagen, Denmark)* 11: 1079 – 1091

Grassart A, Cheng AT, Hong SH, Zhang F, Zenzer N, Feng Y, Briner DM, Davis GD, Malkov D, Drubin DG (2014) Actin and dynamin2 dynamics and interplay during clathrin-mediated endocytosis. *J Cell Biol* 205: 721 – 735

Harding C, Heuser J, Stahl P (1983) Receptor-mediated endocytosis of transferrin and recycling of the transferrin receptor in rat reticulocytes. *J Cell Biol* 97: 329 – 339

Harper CB, Martin S, Nguyen TH, Daniels SJ, Lavidis NA, Popoff MR, Hadzic G, Mariana A, Chau N, McCluskey A, Robinson PJ, Meunier FA (2011) Dynamin inhibition blocks botulinum neurotoxin type A endocytosis in neurons and delays botulism. *J Biol Chem* 286: 35966 – 35976

Hémar A, Lieb M, Subtil A, DiSanto JP, Dautry-Varsat A (1994) Endocytosis of the β chain of interleukin 2 receptor requires neither interleukin 2 nor the γ chain. *Eur J Immunol* 24: 1951 – 1955

Hémar A, Subtil A, Lieb M, Morelon E, Hellio R, Dautry-Varsat A (1995) Endocytosis of interleukin 2 receptors in human T lymphocytes: distinct intracellular localization and fate of the receptor α, β and γ chains. *J Cell Biol* 129: 55 – 64

Henne WM, Boucrot E, Meinecke M, Evergren E, Vallis Y, Mittal R, McMahon HT (2010) FCHo proteins are nucleators of clathrin-mediated endocytosis. *Science (New York, NY)* 328: 1281 – 1284

Howes MT, Kirkham M, Riches J, Cortese K, Walser PJ, Simpson F, Hill MM, Jones A, Lundmark R, Lindsay MR, Hernandez-Deviez DJ, Hadzic G, McCluskey A, Bashir R, Liu L, Pilch P, McMahon H, Robinson PJ, Hancock JF, Mayor S *et al* (2010a) Clathrin-independent carriers form a high capacity endocytic sorting system at the leading edge of migrating cells. *J Cell Biol* 190: 675 – 691

Howes MT, Mayor S, Parton RG (2010b) Molecules, mechanisms, and cellular roles of clathrin-independent endocytosis. *Curr Opin Cell Biol* 22: 519 – 527

Karnovsky M (1971) Use of ferrocyanide reduced osmium tetroxide in electron microscopy. *Ann Meet Am Soc Cell Biol, New Orleans, Louisiana*, p146

Kessels MM, Qualmann B (2002) Syndapins integrate N-WASP in receptor-mediated endocytosis. *EMBO J* 21: 6083 – 6094

Krause M, Gautreau A (2014) Steering cell migration: lamellipodium dynamics and the regulation of directional persistence. *Nat Rev Mol Cell Biol* 15: 577 – 590

Lamaze C, Dujeancourt A, Baba T, Lo C, Benmerah A, Dautry-Varsat A (2001) Interleukin 2 receptors and detergent-resistant membrane domains define a clathrin-independent endocytic pathway. *Mol Cell* 7: 661 – 671

Lebensohn AM, Kirschner MW (2009) Activation of the WAVE complex by coincident signals controls actin assembly. *Mol Cell* 36: 512 – 524

Lim JP, Gleeson PA (2011) Macropinocytosis: an endocytic pathway for internalising large gulps. *Immunol Cell Biol* 89: 836 – 843

Macia E, Ehrlich M, Massol R, Boucrot E, Brunner C, Kirchhausen T (2006) Dynasore, a cell-permeable inhibitor of dynamin. *Dev Cell* 10: 839 – 850

McMahon HT, Boucrot E (2011) Molecular mechanism and physiological functions of clathrin-mediated endocytosis. *Nat Rev Mol Cell Biol* 12: 517 – 533

Menon M, Schafer DA (2013) Dynamin: expanding its scope to the cytoskeleton. *Int Rev Cell Mol Biol* 302: 187 – 219

Merrifield CJ, Feldman ME, Wan L, Almers W (2002) Imaging actin and dynamin recruitment during invagination of single clathrin-coated pits. *Nat Cell Biol* 4: 691 – 698

Mooren OL, Galletta BJ, Cooper JA (2012) Roles for actin assembly in endocytosis. *Annu Rev Biochem* 81: 661 – 686

Mousavi SA, Malerod L, Berg T, Kjeken R (2004) Clathrin-dependent endocytosis. *Biochem J* 377: 1 – 16

Oikawa T, Yamaguchi H, Itoh T, Kato M, Ijuin T, Yamazaki D, Suetsugu S, Takenawa T (2004) PtdIns(3,4,5)P3 binding is necessary for WAVE2-induced formation of lamellipodia. *Nat Cell Biol* 6: 420 – 426

Reider A, Barker SL, Mishra SK, Im YJ, Maldonado-Baez L, Hurley JH, Traub LM, Wendland B (2009) Syp1 is a conserved endocytic adaptor that contains domains involved in cargo selection and membrane tubulation. *EMBO J* 28: 3103 – 3116

Sandvig K, Pust S, Skotland T, van Deurs B (2011) Clathrin-independent endocytosis: mechanisms and function. *Curr Opin Cell Biol* 23: 413 – 420

Sauvonnet N, Dujeancourt A, Dautry-Varsat A (2005) Cortactin and dynamin are required for the clatrin-independent endocytosis of γc cytokine receptor. *J Cell Biol* 168: 155 – 163

Shevchuk AI, Novak P, Taylor M, Diakonov IA, Ziyadeh-Isleem A, Bitoun M, Guicheney P, Lab MJ, Gorelik J, Merrifield CJ, Klenerman D, Korchev YE (2012) An alternative mechanism of clathrin-coated pit closure revealed by ion conductance microscopy. *J Cell Biol* 197: 499 – 508

Sigismund S, Confalonieri S, Ciliberto A, Polo S, Scita G, Di Fiore PP (2012) Endocytosis and signaling: cell logistics shape the eukaryotic cell plan. *Physiol Rev* 92: 273 – 366

Steffen A, Rottner K, Ehinger J, Innocenti M, Scita G, Wehland J, Stradal TE (2004) Sra-1 and Nap1 link Rac to actin assembly driving lamellipodia formation. *EMBO J* 23: 749 – 759

Subtil A, Hémar A, Dautry-Varsat A (1994) Rapid endocytosis of interleukin 2 receptors when clathrin-coated pit endocytosis is inhibited. *J Cell Sci* 107: 3461 – 3468

Subtil A, Delepierre M, Dautry-Varsat A (1997) An α-helical signal in the cytosolic domain of the interleukin 2 receptor β chain mediates sorting towards degradation after endocytosis. *J Cell Biol* 136: 583 – 595

Taylor MJ, Perrais D, Merrifield CJ (2011) A high precision survey of the molecular dynamics of Mammalian clathrin-mediated endocytosis. *PLoS Biol* 9: e1000604

Wu M, Huang B, Graham M, Raimondi A, Heuser JE, Zhuang X, De Camilli P (2010) Coupling between clathrin-dependent endocytic budding and F-BAR-dependent tubulation in a cell-free system. *Nat Cell Biol* 12: 902 – 908

Xu X, Johnson P, Mueller SC (2009) Breast cancer cell movement: imaging invadopodia by TIRF and IRM microscopy. *Methods Mol Biol* 571: 209 – 225